Vibrational Spectroscopy 81 (2015) 112–118

Contents lists available at ScienceDirect

Vibrational Spectroscopy

journal homepage: www.elsevier.com/locate/vibspec

Raman spectroscopic studies of $CuFeO_2$ at high pressures

Nilesh P. Salke[a], K. Kamali[b], T.R. Ravindran[b], G. Balakrishnan[c], Rekha Rao[a,*]

[a] Solid State Physics Division, Bhabha Atomic Research Centre, Mumbai, 400085, India
[b] Materials Science Group, Indira Gandhi Centre for Atomic Research, Kalpakkam, 603102, India
[c] Department of Physics, University of Warwick, Coventry CV4 7AL, United Kingdom

ARTICLE INFO

Article history:
Received 25 August 2015
Received in revised form 19 October 2015
Accepted 28 October 2015
Available online 2 November 2015

Keywords:
Raman spectroscopy
High pressure
Phase transition
Delafossite

ABSTRACT

Structural stability of a multiferroic compound $CuFeO_2$ belonging to the delafossite family has been investigated at high pressures using *in-situ* Raman spectroscopy. At ambient conditions, $CuFeO_2$ has a rhombohedral structure with space group $R\bar{3}m$. It has two Raman active modes, identified as E_g and A_{1g}. Both Raman mode frequencies harden with pressure. At 18 GPa, the doubly degenerate mode E_g splits, followed by softening of one of the split components. This is also accompanied by rapid softening of the high frequency mode. Features observed across 18 GPa confirm the reported structural phase transition. Beyond 23 GPa, there is an abrupt loss of Raman intensity and no Raman spectra could be recorded. This could be due to another structural transition. Raman spectroscopic data in the first high pressure phase give evidence for rearrangement in the FeO_6 octahedra which eventually leads to an increased coordination of copper in the second high pressure phase. Using the temperature dependence and the present pressure dependence of Raman mode frequencies of $CuFeO_2$, implicit and explicit contributions to their anharmonicity in the ambient phase are separated. The Raman spectroscopic data are correlated with available structural data for the delafossite family of compounds.

1. Introduction

The delafossite family of compounds with general formula AMO_2 (A = Cu, Ag, M = Al, Ga, La, Fe, Cr) have been studied exclusively due to their technological applications such as solar cell, touch panels and ultraviolet diodes [1]. These compounds have a layered structure in which monovalent cations A (A = Cu, Ag) are linearly coordinated with two oxygen ions along the c-axis and the trivalent cations M are octahedrally coordinated to oxygen atoms; these compounds belong to space group hexagonal $P6_3/mmc$ or rhombohedral $R\bar{3}m$ space group depending on the stacking along the c-direction. Many of the delafossite family compounds are transparent conducting oxides (TCO) with p-type conductivity [1,2]. TCOs are important in technological applications due to a rare combination of electrical conductivity and optical transparency. Most of the reported TCOs like SnO_2, ZnO and In_2O_3 have n-type conductivity. Therefore p-type conductivity found in delafossite is rare and plays an essential role in forming transparent p–n junctions for various applications. Some copper delafossites are also reported to show anisotropic negative thermal expansion (NTE) at low temperatures, where perpendicular vibrations of Cu atom in O—Cu—O bond are considered responsible for NTE behavior [3]. Delafossite compounds where the octahedrally coordinated trivalent cation has a magnetic moment, as in $CuFeO_2$ or $CuCrO_2$, also exhibit multiferroic properties [4]. $CuFeO_2$ is a triangular lattice antiferromagnet which is known to show magnetoelectric and magnetoelastic effects due to geometric frustration [5]. It exhibits interesting magnetic phase transitions and spontaneous spin-lattice coupling which has been studied extensively [6,7]. $CuFeO_2$ doped with Sn and Ni has been explored for thermoelectric properties as well [8,9]. $CuFeO_2$ has also been explored recently for various applications such as hydrogen production [10–11], as a hetero-junction diode [12], as anode in lithium ion batteries [13] and for gas sensing [14].

High pressures studies of materials are of inherent interest as pressure is considered as a clean perturbation. Many delafossites have been studied under pressure in order to explore their physical properties and phase stability. $CuFeO_2$ has been investigated at high pressures to understand its magnetic behavior at high pressures [15–17]. High pressure neutron diffraction studies of $CuFeO_2$ have been performed to explore pressure induced magnetic phase transitions [15]. It has also been reported that the magnetic long range order is suppressed at a pressure of 7.9 GPa [16]. From Mossbauer spectroscopy at high pressures it was reported that above 18 GPa antiferromagnetic order stabilized at

* Corresponding author. Fax: +91 22 25505141.
E-mail address: rekhar@barc.gov.in (R. Rao).

http://dx.doi.org/10.1016/j.vibspec.2015.10.010

$T < T_N$ [17]. Recent X-ray diffraction studies on $CuFeO_2$ revealed a sequence of structural phase transitions- first at 18 GPa to a monoclinic phase of space group $C2/c$ accompanied by an onset of long range ferromagnetic order. Above 23 GPa, transformation to $P\bar{3}m$ begins, in which charge transfer takes place between Fe–Cu [18]. At around 23 GPa, a valence transition was observed where Fe^{3+} was partially transformed to Fe^{2+} and Cu^{+1} transformed to Cu^{+2}. The $P\bar{3}m$ phase was found to consist of distorted tetrahedra around copper. Many other members of the delafossite family of compounds like $CuGaO_2$, $CuAlO_2$, $CuCrO_2$ and $CuLaO_2$ have also been explored at high pressures using X-ray diffraction and Raman spectroscopy to understand their phase stability [19–25]. Among them, $CuAlO_2$ [21] and $CuLaO_2$ [24] have some similarity in high pressure behavior with the high pressure phase having additional low frequency modes which are attributed to a structure with two molecules per unit cell in $CuAlO_2$ [22]. All these delafossites show splitting of E_g mode across the high pressure transition indicating lowering of symmetry. Raman spectroscopic studies on $CuAlO_2$ and $CuCrO_2$ showed that there is a softening of the high frequency mode in the high pressure phase [21,25]. *Ab initio* phonon calculations of $CuGaO_2$ and $CuAlO_2$ showed that dynamical instability arises in acoustic modes under pressure which is possibly related to a phase transition [20,21].

One common feature in the high pressure behavior of copper delafossites is the anisotropy of compression, with the *a*-axis being more compressible than the *c*-axis which is typical of this family. It was reported from EXAFS measurements on $CuAlO_2$ that there is a change in copper environment in the high pressure phase [22]. In $CuAlO_2$ and $CuGaO_2$, there is a gradual reduction of Cu-O distance in the ambient phase under compression and a gradual enlargement of Cu—O distance beyond the transition pressure. Also the Ga—O distance is unaffected by the transition in $CuGaO_2$. In contrast to this, in $CuFeO_2$ it is found that though there is a gradual reduction of Cu—O bond-length in the ambient phase, there is a discontinuous enhancement at the first transition followed by a gradual reduction at high pressures. This is observed across the second structural transition also. On the other hand Fe-O distances are found to compress continuously upto the second transition pressure at which there is a discontinuous enhancement due to Fe^{3+}–Fe^{2+} valence transformation. Because of the interplay between structural changes, magnetic properties and charge transfer in magnetic compounds, which are absent in $CuAlO_2$ or $CuGaO_2$, high pressure structures of delafossites are different. In the case of $CuCrO_2$, high pressure Raman spectroscopic studies have identified a reversible structural transition around 23 GPa tentatively to an ordered rocksalt type structure. In all these structural transitions of delafossite under high pressures, Raman spectroscopy has played an important role confirming structural information and revealing information about the changes in the local coordination across the transition. Here, we report our *in-situ* Raman spectroscopic investigations of $CuFeO_2$ at high pressures to understand the behavior of phonons across the reported structural phase transitions and correlate the observed behavior to the available XRD data. Temperature dependent Raman spectroscopic measurements are also carried out to estimate the anharmonicity of Raman modes. Implicit and explicit anharmonicity of vibrational modes are separated using the pressure and temperature dependence of the Raman mode frequencies. The observed Raman spectra as well as high pressure behavior of $CuFeO_2$ is compared with available data on other copper delafossite compounds to correlate the structural parameters with Raman data.

2. Experimental details

Single crystals of $CuFeO_2$ grown by floating zone technique were used for the current studies [26]. *In-situ* high pressure Raman spectra of unoriented single crystal pieces of $CuFeO_2$ are recorded up to 23 GPa from a symmetric diamond anvil cell (DAC) with diamonds of culet diameter 500 μm, using a micro Raman spectrometer (Renishaw, UK, model inVia) with 514.5 nm laser

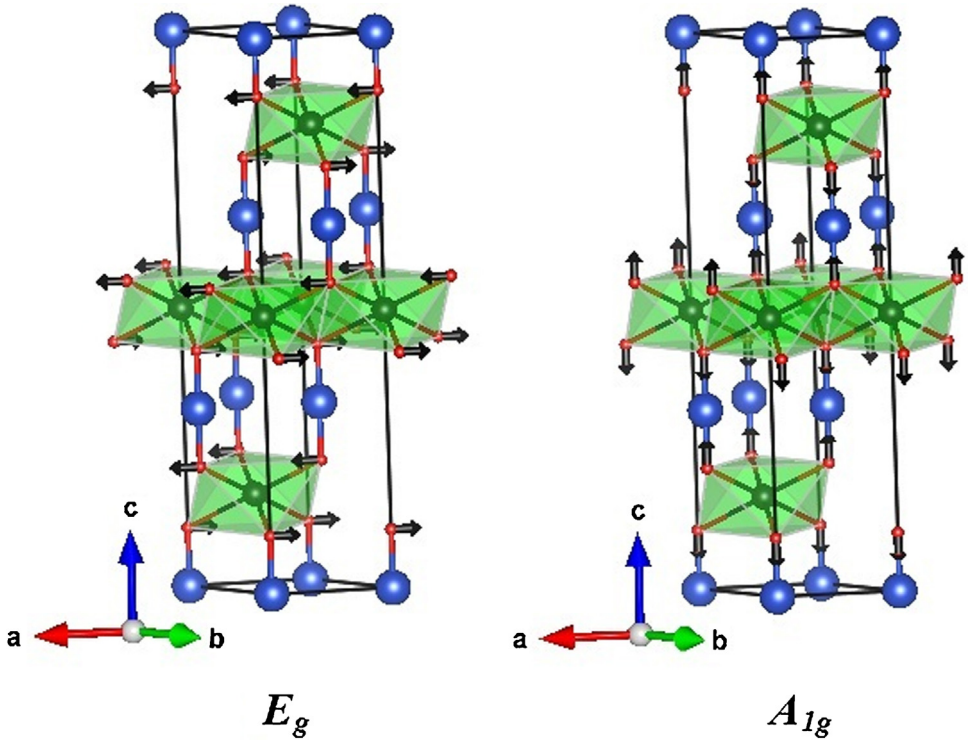

Fig. 1. Eigen vectors for E_g and A_{1g} modes of vibration in $CuMO_2$ delafossite compounds. (Symbols: red—Oxygen, green—trivalent *M* cation, blue—Copper). (For interpretation of the references to colour in this figure legend, the reader is referred to the web version of this article.)

excitation. 4:1 mixture of methanol-ethanol was used as pressure transmitting medium, which remains hydrostatic up to 10 GPa beyond which it becomes non-hydrostatic [27]. Pressure calibration was done by ruby fluorescence method [27]. Low temperature Raman measurements was carried out using 532 nm laser excitation focused to a spot size of 20 μm and scattered light was analyzed using a home built 0.9 m single monochromator, coupled with an edge filter and detected by a cooled CCD (ANDOR Technology). Spectral resolution of both the Raman instruments in the measured range is 1.5 cm^{-1}/pixel. Reproducibility of the spectra is within ±0.2 cm^{-1}. Low temperature Raman spectra was recorded down to 80 K using the temperature stage Linkam THMS 600.

3. Results and discussion

Delafossites of CuMO_2 family crystallize in a rhombohedral structure with space group $R\bar{3}m$ (Phase I). It consists of one formula unit per primitive cell resulting in 12 normal modes of vibration which transform as $\Gamma = A_{1g} + E_g + 3A_{2u} + 3E_u$ of which E_g and A_{1g} are Raman active modes. Fig. 1 shows the eigenvectors corresponding to E_g and A_{1g} modes for the CuMO_2 family. Copper and trivalent cation M are at rest and oxygen atoms vibrate in Raman active modes. Vibrations in the direction of Cu—O bonds along the c-axis are represented by A modes, whereas vibrations in the direction perpendicular to c-axis correspond to E modes. Since Raman mode frequency is inversely proportional to the bond length and to square root of the reduced mass of the vibrating atoms, we have compared the Raman mode frequencies of different copper delafossites with various structural parameters such as Cu—O, M—O bond-length and inverse square root of the reduced atomic mass of Cu atom and MO_6 octahedra [28], and correlated them to identify the nature of Raman mode frequencies. Table 1 contains structural parameters and the Raman mode frequencies for various delafossite compounds. As seen in the Table 1, Raman mode frequency varies inversely with the M—O bond lengths in this family. We have plotted Raman mode frequency of E_g and A_{1g} mode for different delafossites as a function of M—O bond-length in Fig. 2(a). We have also plotted Raman mode frequencies against inverse square root of reduced atomic mass of Cu atom and MO_6 octahedra in Fig. 2(b) which is found to behave nearly linear. This observation indicates that though the Raman mode vibrations E_g and A_{1g} in the ambient delafossite structure are along the Cu—O bond and perpendicular to Cu—O bond respectively, the magnitude of frequencies E_g and A_{1g} have significant effect due to the octahedral cation M. It also points to dependence of Raman frequencies on M—O bond-length which in turn would depend on M^{3+} ionic radius.

As the Raman frequencies depend on bond-length, which in turn depends on radii of octahedrally coordinated trivalent cations, we have correlated the bond-length and other structural parameters like lattice parameter and volume with radii of M cation for the delafossites. In Fig. 3(a), Cu—O and M—O bond-lengths are plotted against ionic radius of M cation. It is seen that M—O bond-length increases drastically with increase in ionic radius of trivalent cation M but there is no appreciable change in Cu—O bond-length as a function of ionic radius of M cation. Hence Cu atom has no chemical pressure generated due to size of trivalent cation M and Cu—O bond is nearly unaffected. Lattice parameters and unit cell volume are also plotted against ionic radius of M cation as shown in Fig. 3(b). Lattice parameter along the a-axis consists of MO_6 octahedral layer whereas c-axis consists of O—Cu—O linkage with alternate layers of MO_6 octahedra. Fig. 3(b) indicates a-parameter in delafossite family is directly proportional to the ionic radius of trivalent cation, whereas c-parameter is nearly unaffected. This observation is consistent with observations of Fig. 3(a). As Cu—O bond-length and c-parameter do not change with trivalent cation size, it implies that thickness of MO_6 octahedral layer remains nearly constant in spite of drastic change in M—O bond-length. Unit cell volume increases with trivalent cation size as shown with open squares in Fig. 3(b), which is purely due to increase in a-axis. These structural details are

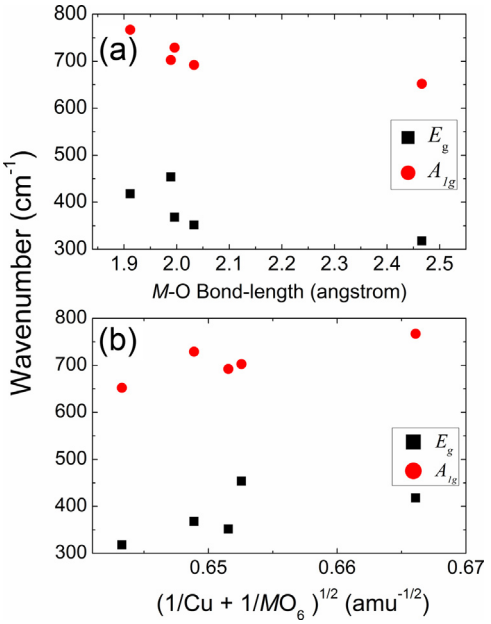

Fig. 2. (a) Variation of Raman mode frequencies with M—O bond-length. Solid circles from left to right are $CuAlO_2$, $CuCrO_2$, $CuGaO_2$, $CuFeO_2$ and $CuLaO_2$ respectively. (b) Variation of Raman mode frequencies with inverse square root of reduced atomic mass of Cu atom and MO_6 octahedra. Solid circles from left to right are $CuLaO_2$, $CuGaO_2$, $CuFeO_2$, $CuCrO_2$ and $CuAlO_2$, respectively. References are mentioned in Table 1.

Table 1
Ionic radius and mass of octahedrally coordinated trivalent cations, Raman mode frequencies, lattice parameters and bond-lengths for various delafossite compounds.

Delafossite	Ionic radii of trivalent cation (Å) [29]	Mass of trivalent cation (amu)	Raman mode frequency		Lattice parameter		Bond-length		Ref.
			E_g (cm^{-1})	A_{1g} (cm^{-1})	a (Å)	c (Å)	Cu—O (Å)	M—O (Å)	
$CuLaO_2$	1.14	138.9055	318	652	3.8326	17.092	1.760	2.466	[24,30]
$CuNdO_2$	1.04				3.7119	17.085	1.836	2.370	[30]
$CuYO_2$	0.92				3.533	17.136	1.827	2.285	[31]
$CuScO_2$	0.81				3.2204	17.0999	1.831	2.121	[2,32]
$CuFeO_2$	0.64	55.845	351.8(2)	692.3(2)	3.0351	17.166	1.835	2.033	[4,33]
$CuCrO_2$	0.63	51.9961	453.54(6)	702.71(8)	2.9767	17.1113	1.8455	1.9890	[25]
$CuGaO_2$	0.62	69.273	368(1)	729(1)	2.977	17.171	1.848	1.996	[19,20,31]
$CuAlO_2$	0.51	26.98154	418.1(1)	767.2(3)	2.8584	16.958	1.8617	1.9116	[21,34]

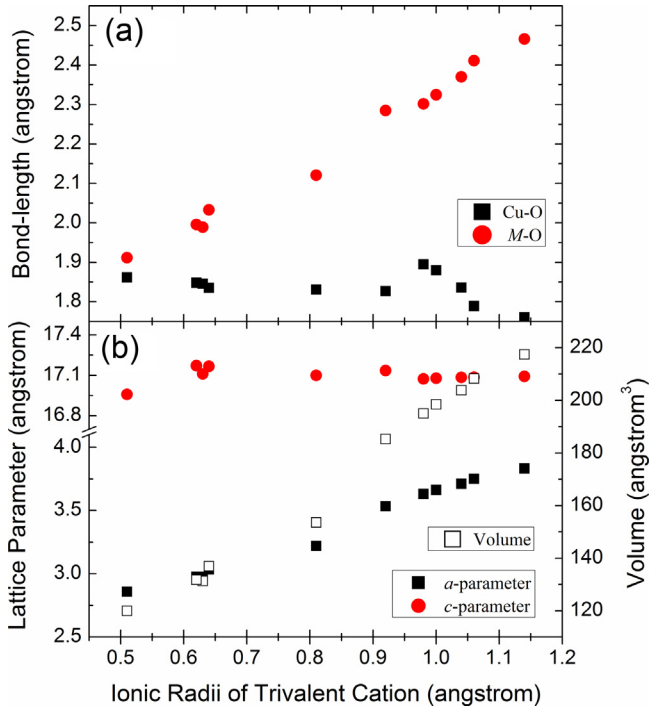

Fig. 3. (a) Variation of Cu-O and *M*-O bond-length with ionic radii of trivalent cation. (b) Variation of lattice parameters and volume with ionic radii of trivalent cation. Symbols from left to right correspond to $CuAlO_2$, $CuGaO_2$, $CuCrO_2$, $CuFeO_2$, $CuScO_2$, $CuYO_2$, $CuNdO_2$ and $CuLaO_2$ respectively. References are mentioned in Table 1.

relevant to the high pressure behavior which will be discussed later.

3.1. Raman spectroscopic studies on $CuFeO_2$ at high pressures

Raman spectra of $CuFeO_2$ have two Raman active modes E_g and A_{1g} at 352 and 692 cm^{-1} respectively, identified from reported polarized Raman measurements [4]. The broad band around 500 cm^{-1} is attributed to relaxation of selection rules by defects such as Cu vacancies, interstitial oxygen's or tetrahedrally coordinated Fe^{3+} on the Cu site [4]. Fig. 4 shows the Raman spectra of $CuFeO_2$ at various pressures. Both Raman mode frequencies harden with increase in pressure; this could be associated with compression of Fe—O bond-length under pressure in phase I, which is consistent with the report suggesting that, *a*-axis which has contribution from Fe—O bond is more compressible than *c*-axis which has contribution from Cu—O bond and also evidenced from increase in *c*/*a* for $CuFeO_2$ in phase I [18]. Compression of Fe—O in phase I also supports the conclusion of Fig. 2, which pointed toward the dependence of Raman mode frequencies on *M*—O bond-lengths in delafossite. At around 18 GPa, the doubly degenerate E_g Raman mode shows splitting across the reported transition to the monoclinic $C2/c$ phase, with one of the split components softening on further compression. There is also a change in pressure dependence of the A_{1g} band around this pressure which tends to soften drastically. Unlike in $CuAlO_2$ and $CuLaO_2$, there are no additional modes in the low frequency region across the transition [21,24]. These additional modes in the low frequency were attributed to the zone-edge phonons in $CuAlO_2$ [22]. The changes observed are indicative of the reported phase transition from $R\bar{3}m$ to $C2/c$ (Phase II) structure at 18 GPa [18]. It may be noted that the splitting of the E_g mode observed across the structural transition is similar to that in other delafossites. In the case of $CuGaO_2$ and $CuLaO_2$,A_{1g} mode disappears after the first transition; it could be either due to weak intensity or may not be allowed due to Raman selection rule in the high pressure phase. While some of the aspects are similar to the other delafossites, there are some differences in the high pressure behavior of $CuFeO_2$. Above 18 GPa, two of the three Raman bands show unusual softening, particularly the high frequency mode softens rapidly. It is indicative of instability which could lead to another phase transition. Softening of the modes observed in phase II suggests that the Fe—O distances are increasing but it contradicts earlier report of decrease of Fe—O bond-length in phase II [18]. However the Fe—O distances mentioned in Ref. [18] are mean distances and it is possible that the splitting of E_g mode observed across the transition could be due to rearrangement of the FeO_6 octahedra resulting in distortion and a few of the Fe—O bond-lengths could be elongating with pressure in the phase II. Cu—O bonds which are almost incompressible in phase I are tilted across the transition and in phase II, Cu—O bonds are more compressible than Fe—O bonds which is also reflected in decrease in *c*/*a* [18]. Softening of the high frequency mode observed after transition is similar to that in $CuAlO_2$ and $CuCrO_2$. Rapid softening of the high frequency mode indicates change in Fe—O bond-length

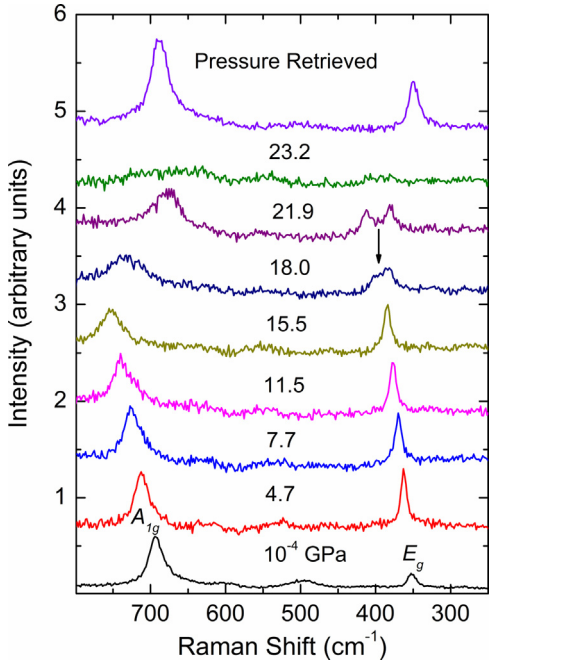

Fig. 4. Raman spectra of $CuFeO_2$ at various pressures. Arrow indicates the splitting of Raman modes at 18 GPa.

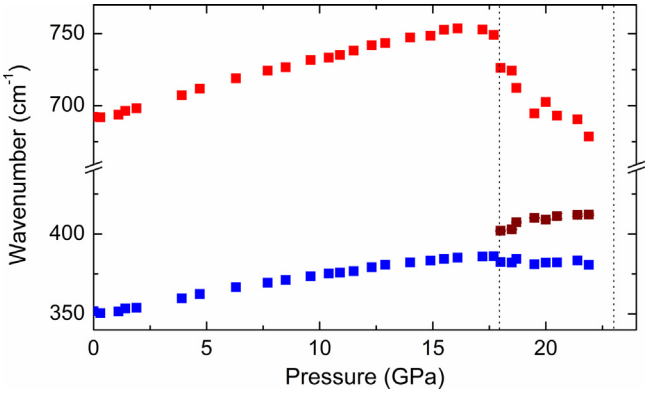

Fig. 5. Pressure dependencies of Raman mode frequencies of $CuFeO_2$. Vertical lines show the transition pressure.

which ultimately results in change in copper coordination leading to the second high pressure transition above 23 GPa. Fig. 5 shows the pressure dependence of Raman mode frequencies. Since the pressure range of phase I is large, pressure dependence of Raman mode frequencies are fitted for quadratic equation given as $\omega(P) = \omega_0 + (A \times P) + (B \times P^2)$. However, pressure dependence of Raman mode frequencies for the phase II have been fitted for a linear equation. Pressure dependant coefficient for Raman mode frequencies in phase I and phase II is given in Table 2. Beyond 23 GPa, there is a loss of Raman intensity and we could not follow any of the Raman modes which is probably due to the second phase transition where there is a charge transfer between Fe and Cu transfer [18] which could also involve a change in band structure. It may be noted that such a loss of intensity has been observed in $CuLaO_2$ also across bandgap collapse [24]. However, loss of Raman intensity beyond 23 GPa do not allow us to infer more about this phase. After releasing the pressure from 23.2 GPa, the original phase of $CuFeO_2$ is recovered.

3.2. Raman spectroscopic studies on $CuFeO_2$ as a function of temperature

Temperature dependent Raman spectroscopic measurements are carried out on $CuFeO_2$ in the temperature range 80–298 K to estimate the anharmonicity of modes which is useful in modeling thermodynamic properties of the material. Fig. 6 shows the Raman spectra of $CuFeO_2$ at various temperatures. Temperature dependence of Raman modes is presented in Fig. 7. Both Raman modes show increase in frequency with decrease in temperature. Temperature dependent coefficient for Raman mode frequencies is given in Table 2. The temperature dependence of phonon frequency at constant pressure for an isotropic system consists of two contributions: (a) due to change in volume-only with temperature, called implicit contribution (or quasiharmonic contribution) and (b) a purely anharmonic contribution (explicit contribution), which arises due to changes in vibrational amplitude [35]. Due to explicit/true anharmonicity one phonon decays into two or three phonons, this process is called as three and four phonon decay process respectively. Explicit anharmonicity term represents the total contribution due to three and four phonon decay process. We have separated the implicit and explicit anharmonicity contributions, using mathematical expression given in Ref. [35]. Pressure and temperature dependence of Raman mode frequencies of $CuFeO_2$ obtained from present experimental work is useful for separating implicit and explicit anharmonicity contributions which are given in Table 2. In the earlier work on polycrystalline $CuFeO_2$ by Pavunny et al. have used isothermal Grüneisen parameter of $CuAlO_2$ for calculating quasiharmonic contribution in the absence of high pressure Raman data of $CuFeO_2$ [36]. Also the temperature dependence of mode frequencies is higher for both the modes probably because of the sample being polycrystalline. From Table 2, it can be seen that, for both the

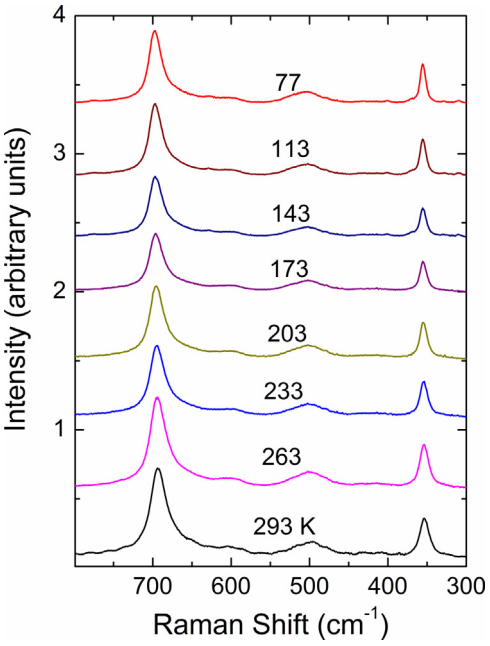

Fig. 6. Raman spectra of $CuFeO_2$ at various temperatures.

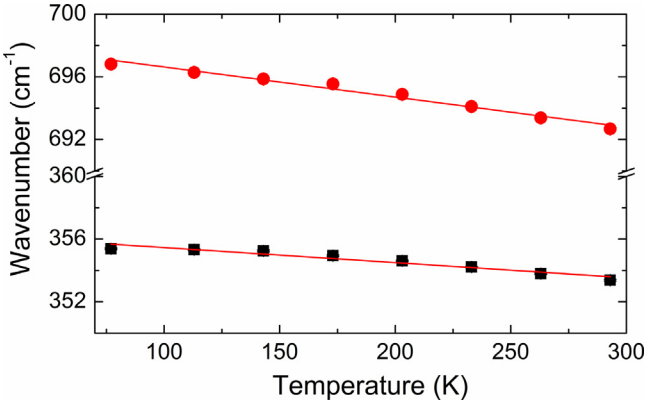

Fig. 7. Temperature dependence of Raman mode frequencies of $CuFeO_2$.

Raman modes, the implicit anharmonicity contribution is dominant in the case of $CuFeO_2$; similar to that for $CuLaO_2$. In $CuFeO_2$, explicit anharmonicity term of E_g mode has positive value which indicates that it has major contribution from four phonon decay process whereas A_{1g} mode has negative value which implies that three phonon decay process is dominant for this mode.

In order to understand the high pressure behavior of delafossite family of compounds, Raman mode frequencies and their pressure

Table 2
Pressure and temperature dependence of Raman mode frequencies for $CuFeO_2$. Implicit and explicit anharmonicity contribution to the total anharmonicity is separated. We have used bulk modulus $B_0 = 148$ GPa [18] and thermal expansion coefficient $\alpha = 2.61 \times 10^{-5}\,K^{-1}$ [36] to separate implicit and explicit anharmonicity.

Raman shift ω (cm^{-1})	Phase I						Phase II $d\omega/dP$ ($cm^{-1}\,GPa^{-1}$)
	A ($cm^{-1}\,GPa^{-1}$)	B ($cm^{-1}\,GPa^{-2}$)	$d\omega/dT$ ($cm^{-1}\,K^{-1}$)	Anharmonicity ($10^{-5}\,K^{-1}$)			
				Total	Implicit	Explicit	
351.8(2) (E_g)	2.90(3)	−0.043(2)	−0.0096(9)	−2.73	−3.18	−0.45	−0.2(1) −3.1(1)
692.3(2) (A_{1g})	4.72(5)	−0.052(1)	−0.019(1)	−2.74	−2.63	−0.11	−12.3(2)

Table 3
Raman mode frequencies, its pressure dependence and isothermal Grüneisen parameter for various delafossites. Isothermal Grüneisen parameter calculated using equation $\gamma_{iT} = (B_0/\omega_i)(\partial\omega_i/\partial P)_T$, where B_0 is bulk modulus.

Delafossite	E_g mode			A_{1g} mode			Ref.
	ω cm^{-1}	dω/dP cm^{-1} GPa^{-1}	γ_{iT}	ω cm^{-1}	dω/dP cm^{-1} GPa^{-1}	γ_{iT}	
$CuLaO_2$	318	5.0	2.42	652	9	2.13	[24]
$CuFeO_2$	351.8(2)	2.90(3)	1.22	692.3(2)	4.72(5)	1.01	This paper
$CuCrO_2$	453.54(6)	2.55	0.88	702.71(8)	4.79	1.07	[25]
$CuGaO_2$	368(1)	2.78	1.53	729(1)	4.64	1.29	[20]
$CuAlO_2$	418.1(2)	2.72	1.3	767.2(3)	4.96	1.29	[21]

dependence and Grüneisen parameter for various copper delafossites are tabulated in Table 3. In delafossite compounds, *a*-axis is more compressible than *c*-axis and hence *c*/*a* increases with pressure [19,22,24,25]. As the vibrations of A_{1g} mode is along the *c*-axis and E_g mode vibrations are perpendicular to the *c*-axis, one can directly compare the mode Grüneisen parameters of the two modes. This is reflected in high pressure Raman spectroscopic data where it is seen that Grüneisen parameter of A_{1g} mode is lower than that of the E_g mode (with the exception of $CuCrO_2$). It has also been observed that, ratio of the pressure dependence of A_{1g} to E_g mode is found to be around 1.8 for all the copper delafossites.

Even though the structural modifications in $CuFeO_2$ and $CuCrO_2$ are expected to be interlinked to magnetic properties, there is a general trend in the high pressure behavior. In Fig. 8 transition pressure for first high pressure phase transition for a delafossite is plotted against ratio of ionic radii of octahedrally coordinated trivalent cation (R_M) to the ionic radii of monovalent cation Cu (R_{Cu}), similar to that in Ref. [38]. Transition pressure is found to vary inversely with R_M/R_{Cu}. Structurally, across the delafossites, as the ionic radius of *M* increases, while the *c*-axis remains nearly same, *a*-axis increases. At high pressures, since *c*-axis is incompressible and *a*-axis has large compressibility, this must be resulting in distortion of the MO_6 octahedra. Larger the ionic radii, higher the polarizability and hence MO_6 octahedra are deformed at much lower pressures. From Fig. 8, we can predict the approximate transition pressure for other delafossite compounds. It appears that the conventional rule that isostructural compounds having different cations will undergo structural transitions at progressively lower pressures as the cation radius increases holds good for delafossite family of compounds.

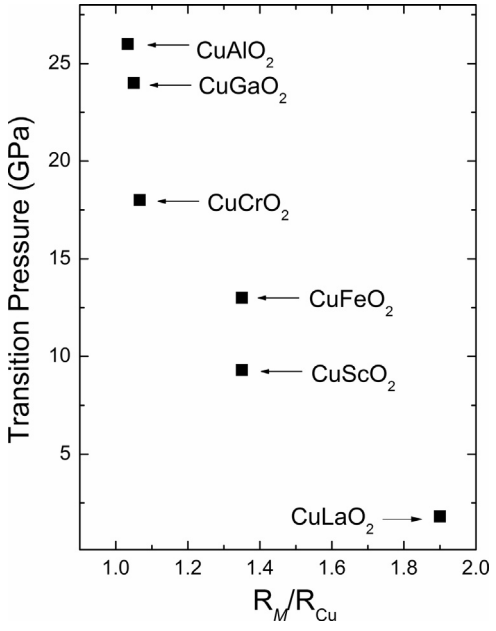

Fig. 8. Variation of transition pressure with ratio of ionic radii of Cu to the ionic radii octahedrally coordinated trivalent cation in delafossite compounds. References are as follows $CuAlO_2$ [21], $CuGaO_2$ [20], $CuCrO_2$ [25], $CuFeO_2$ [18], $CuScO_2$ [37], and $CuLaO_2$ [24].

4. Conclusion

Raman spectroscopic investigations of $CuFeO_2$ are carried out at high pressures up to 23 GPa. In addition to confirming the reported structural transitions, the present results indicate softening of A_{1g} phonon in the first high pressure phase leading to a higher coordination of the copper atom in the second high pressure phase. Separation of anharmonicity components of Raman modes suggests that implicit anharmonicity is dominant in $CuFeO_2$. A survey of the structure and Raman spectroscopic data of the delafossite compounds $CuMO_2$ suggests that there is a correlation between Raman mode frequency and the *M*—O bond-length. The present results will be useful to predict transition pressures as well as to understand the nature of transitions in copper delafossites.

Acknowledgment

Authors are thankful to Dr. S. L. Chaplot and Dr. R. Mukhopadhyay for support and encouragement. Authors thank Mr. M. K. Gupta for providing eigen vectors. NPS acknowledges Department of Atomic energy, India for fellowship support. The work at the University of Warwick was supported by the EPSRC, UK.

References

[1] A.N. Banerjee, K.K. Chattopadhyay, Prog. Cryst. Growth Charact. Mater. 50 (2005) 52.
[2] H. Kawazoe, M. Yasukawa, H. Hyodo, M. Kurita, H. Yanagi, H. Hosono, Nature 389 (1997) 939.
[3] J. Li, A.W. Sleight, C.Y. Jones, B.H. Toby, J. Solid State Chem. 178 (2005) 285.
[4] O. Aktas, K.D. Truong, T. Otani, G. Balakrishnan, M.J. Clouter, T. Kimura, G. Quirion, J. Phys.: Condens. Matter 24 (2012) 036003.
[5] T. Kimura, J.C. Lashley, A.P. Ramirez, Phys. Rev. B 73 (2006) 220401R.
[6] N. Terada, Y. Narumi, Y. Sawai, K. Katsumata, U. Staub, Y. Tanaka, A. Kikkawa, T. Fukui, K. Kindo, T. Yamamoto, R. Kanmuri, M. Hagiwara, H. Toyokawa, T. Ishikawa, H. Kitamura, Phys. Rev. B 75 (2007) 224411.
[7] G. Quirion, M.J. Tagore, M.L. Plumer, O.A. Petrenko, Phys. Rev. B 77 (2008) 094111.
[8] C. Ruttanapun, P. Jindajitawat, W. Thowladda, W. Neeyakorn, C. Thanachayanont, A. Charoenphakdee, Adv. Mater. Res. 802 (2013) 17.
[9] J.-S. Kang, D.H. Kim, J. Hwang, E. Lee, T. Nozaki, K. Hayashi, T. Kajitani, B.-G. Park, J.-Y. Kim, B.I. Min, App. Phys. Lett. 99 (2011) 012108.
[10] C.G. Read, Y. Park, K.S. Choi, J. Phys. Chem. Lett. 3 (2012) 1872.
[11] A. Derbal, S. Omeiri, A. Bouguelia, M. Trari, Int. J. Hydrogen Energy 33 (2008) 4274–4282.
[12] T. Gaewdang, N. Wongcharoen, Adv. Mater. Res. 931-932 (2014) 122–126.
[13] Y. Dong, C. Cao, Y.S. Chui, J.A. Zapien, Chem. Commun. 50 (2014) 10151–10154.
[14] J. Patzsch, I. Balog, P. Krauß, C.W. Lehmann, J.J. Schneider, RSC Adv. 4 (2014) 15348.
[15] N. Terada, D.D. Khalyavin, P. Manuel, T. Osakabe, P.G. Radaelli, H. Kitazawa, Phys. Rev. B 89 (2014) 220403(R).

[16] N. Terada, T. Osakabe, H. Kitazawa, Phys. Rev. B (83) (2011) 020403(R).
[17] W.M. Xu, M.P. Pasternak, R.D. Taylor, Phys. Rev. B 69 (2004) 052401.
[18] W.M. Xu, G.Kh. Rozenberg, M.P. Pasternak, M. Kertzer, A. Kurnosov, L.S. Dubrovinsky, S. Pascarelli, M. Muñoz, M. Vaccari, M. Hanfland, R. Jeanloz, Phys. Rev. B 81 (2010) 104110.
[19] J. Pellicer-Porres, A. Segura, Ch. Ferrer-Roca, D. Martínez-García, J.A. Sans, E. Martínez, J.P. Itié, A. Polian, F. Baudelet, A. Muñoz, P. Rodríguez-Hernández, P. Munsch, Phys. Rev. B 69 (2004) 024109.
[20] J. Pellicer-Porres, A. Segura, E. Martínez, A.M. Saitta, A. Polian, J.C. Chervin, B. Canny, Phys. Rev. B 72 (2005) 064301.
[21] J. Pellicer-Porres, D. Martínez-García, A. Segura, P. Rodríguez-Hernández, A. Muñoz, J.C. Chervin, N. Garro, D. Kim, Phys. Rev. B 74 (2006) 184301.
[22] J. Pellicer-Porres, A. Segura, Ch. Ferrer-Roca, A. Polian, P. Munsch, D. Kim, J. Phys.: Condens. Matter 25 (2013) 115406.
[23] T. Aoyama, A. Miyake, T. Kagayama, K. Shimizu, T. Kimura, Phys. Rev. B 87 (2013) 094401.
[24] N.P. Salke, A.B. Garg, R. Rao, S.N. Achary, M.K. Gupta, R. Mittal, A.K. Tyagi, J. App. Phys. 115 (2014) 133507.
[25] A.B. Garg, A.K. Mishra, K.K. Pandey, S.M. Sharma, J. App. Phys. 116 (2014) 133514.
[26] O.A. Petrenko, G. Balakrishnan, M.R. Lees, D. McK, Paul A. Hoser, Phys. Rev. B 62 (2000) 8983.
[27] G.J. Piermarini, S. Block, J.D. Barnett, J. Appl. Phys. 44 (1973) 5377.
[28] J. Ruiz-Fuertes, D. Errandonea, S. López-Moreno, J. González, O. Gomis, R. Vilaplana, F.J. Manjón, A. Muñoz, P. Rodríguez-Hernández, A. Friedrich, I.A. Tupitsyna, L.L. Nagornaya, Phys. Rev. B 83 (2011) 214112.
[29] R.D. Shannon, C.T. Prewitt, Acta. Cryst. B 25 (1969) 925.
[30] N. Miyasaka, Y. Doi, Y. Hinatsu, J. Solid State Chem. 182 (2009) 2104–2110.
[31] A. Buljan, P. Alemany, E. Rui, J. Phys. Chem. B 103 (1999) 8060–8066.
[32] J. Li, A.F.T. Yokochi, A.W. Sleight, Solid State Sci. 6 (2004) 831–839.
[33] C.T. Prewitt, R.D. Shannon, D.B. Rogers, Inorg. Chem. 10 (1971) 719.
[34] T. Ishiguro, N. Ishizawa, N. Mizutani, M. Kato, J. Solid State Chem. 41 (1982) 132–137.
[35] P.S. Peercy, B. Morosin, Phys. Rev. B 7 (1973) 2779.
[36] S.P. Pavunny, A. Kumar, R.S. Katiyar, J. Appl. Phys. 107 (2010) 013522.
[37] S. Gilliland, J. Pellicer-Porres, A. Segura, A. Muñoz, P. Rodríguez-Hernández, D. Kim, M.S. Lee, T.Y. Kim, Phys. Stat. Sol. (b) 244 (1) (2007) 309–314.
[38] D. Errandonea, F.J. Manjón, Prog. Mater. Sci. 53 (2008) 711–773.